



# A Revision of the Sb-Te Binary Phase Diagram and Crystal Structure of the Modulated $\gamma$ -Phase Field

Stefan Solé<sup>1</sup> · Clemens Schmetterer<sup>2</sup> · Klaus W. Richter<sup>1</sup>

Submitted: 2 March 2022 / in revised form: 6 April 2022 / Accepted: 9 April 2022 / Published online: 2 May 2022  
© The Author(s) 2022

**Abstract** A new experimental study of Sb-Te, based on long term annealed samples homogenized by intermediate powdering and re-annealing of the pressed powder pellets was performed. More than 25 samples were prepared, covering the entire composition range between 0 and 60 at.% Te. This part of the phase diagram was disputed for many years, as the number of phases and their crystal structures were uncertain. Samples were characterized by optical microscopy, SEM/EDX, powder XRD and DTA. Our results show the existence of a continuous single phase field ( $\gamma$ ) ranging from 11.4 to 56.9 at.% Te at 520 °C. A comparison of all obtained diffraction patterns showed clear evidence for a continuously modulated crystal structure. It was possible to refine all powder patterns by applying a structural model in the (3 + 1)-dimensional super-space group R-3m(0,0, $\gamma$ ). Lattice parameters of the basic cell as well as the modulation vector are varying continuously throughout the phase field and the  $\gamma_q$ -component ( $\mathbf{q} = \gamma_q \cdot \mathbf{c}^*$ ) of the incommensurate  $\mathbf{q}$ -vector shows a linear extrapolation to pure Sb ( $\gamma_q = 3/2$ ) and Sb<sub>2</sub>Te<sub>3</sub> ( $\gamma_q = 6/5$ ). In agreement with previous authors, the single-

phase field  $\gamma$  was found to have a melting point minimum (30 at.% Te, 535 °C). Furthermore, two peritectic reactions were observed and the course of liquidus lines was determined in the whole investigated composition range. The new phase diagram differs considerably from all previous versions, and, for the first time, gives a complete rationalization of the crystal structures observed in the debated composition area.

**Keywords** crystal structure · phase diagram · Sb-Te

## 1 Introduction and Literature Review

Antimony-Tellurides, in particular the compound Sb<sub>2</sub>Te<sub>3</sub>, were studied intensively in the last decades because of their potential in various fields of applications. When doped with a suitable dopant, Sb<sub>2</sub>Te<sub>3</sub> can be transformed into both *p*-type and *n*-type semiconductors and has a high potential for various thermoelectric applications.<sup>[1, 2]</sup> In combination with Ge and In it is used as phase change material for random access memory,<sup>[3]</sup> or as base material for optical disc memory.<sup>[4]</sup> Furthermore, Sb<sub>2</sub>Te<sub>3</sub> is a topological insulator which was studied for various advanced applications.<sup>[5, 6]</sup>

Despite the considerable interest in Antimony-Tellurides, the phase diagram Sb-Te is still not well understood. The relevant literature up to the year 1992 was assessed by Ghosh.<sup>[7]</sup>

According to this assessment, shown in Fig. 1, the compound Sb<sub>2</sub>Te<sub>3</sub> shows a congruent melting point at 617.7 °C and a homogeneity range of less than 1 at.%. A eutectic reaction between Sb<sub>2</sub>Te<sub>3</sub> and Te occurs at 422 °C. The composition region between Sb and Sb<sub>2</sub>Te<sub>3</sub> is more

This invited article is part of a special tribute issue of the Journal of Phase Equilibria and Diffusion dedicated to the memory of former JPED Editor-in-Chief John Morral. The special issue was organized by Prof. Yongho Sohn, University of Central Florida; Prof. Ji-Cheng Zhao, University of Maryland; Dr. Carelyn Campbell, National Institute of Standards and Technology; and Dr. Ursula Kattner, National Institute of Standards and Technology.

✉ Klaus W. Richter  
klaus.richter@univie.ac.at

<sup>1</sup> Department of Inorganic Chemistry – Functional Materials, University of Vienna, Vienna, Austria

<sup>2</sup> Department of Physical Chemistry, University of Vienna, Vienna, Austria

complex. Melting in this large composition area (0–60 at.% Te) occurs in the small temperature range of 544–557 °C and single phase samples were found in a large part of the composition range. Based on the work of Abrikosov et al.<sup>[8]</sup> and early crystal structure studies, Ghosh<sup>[7]</sup> proposed the existence of two separate phases fields  $\gamma$  (41–49 at.% Te) and  $\delta$  (16–37 at.% Te) with rhombohedral ( $\gamma$ ) and primitive trigonal ( $\delta$ ) crystal structures. The  $\delta$ -phase was found to show a melting point minimum at 27.7 at.% Te and three additional peritectic reactions were proposed in the composition range between 0 and 60 at.% Te. Invariant reactions according to Ghosh<sup>[7]</sup> are summarized in Table 1.

In a following work, based on the assessment of Ghosh,<sup>[7]</sup> Shelimova et al.<sup>[9]</sup> propose the existence of several layered superstructures based on the structure of Sb (As-type) between 30 and 56 at.% Te. These superstructures are refineable only at their specific composition, even though some of them occur in an extended single-phase

field. Two compounds were prepared in by Shelimova et al.,<sup>[9]</sup> others taken from existing literature.<sup>[10]</sup> The proposed phase diagram agrees with Ghosh<sup>[7]</sup> and Abrikosov,<sup>[8]</sup> having two separate single-phase fields  $\gamma$  and  $\delta$ . Crystallographic data for Sb-Te phases for the following discussions are summarized in Table 2.

A thermodynamic assessment using the CALPHAD method, also based on the work by Ghosh,<sup>[7]</sup> was done by Guo et al.<sup>[16]</sup> who reproduced the classically assessed phase diagram in Ref. 7. Another experimental work by Eckerlin and Stegherr<sup>[17]</sup> is in line with the phase diagram from Abrikosov,<sup>[8]</sup> but the authors state that they can only verify one peritectic reaction between 30 and 60 at.% Te. Furthermore, they could not confirm the  $\gamma$ -phase described by Abrikosov,<sup>[8]</sup> while also discussing at least 11 discrete phases in this range.

A different approach, suggesting only one broad phase field between Sb and  $Sb_2Te_3$ , is also supported by some authors. Brown and Lewis<sup>[18]</sup> proposed a phase diagram

**Fig. 1.** The Sb-Te phase diagram according to the assessment of Ghosh<sup>[7]</sup>

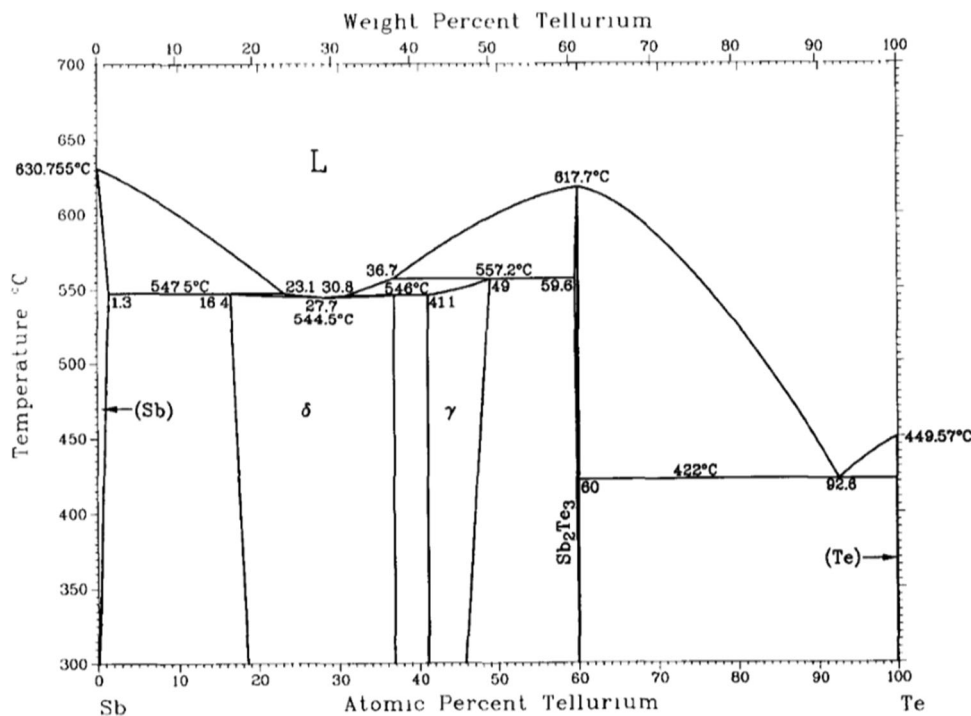


**Table 1.** Invariant reactions in Sb-Te according to Ghosh<sup>[7]</sup>

Reaction	Composition, at.% Sb		Temp., °C	Reaction type
$L \leftrightarrow Sb$		100	630.75	Melting
$L + (Sb) \leftrightarrow \delta$	76.9	98.7	547.35	Peritectic
$L \leftrightarrow \delta$	72.3	72.3	544.35	Congruent
$L + \gamma \leftrightarrow \delta$	69.2	58.9	545.85	Peritectic
$L + Sb_2Te_3 \leftrightarrow \gamma$	63.3	40.4	557.05	Peritectic
$L \leftrightarrow Sb_2Te_3 + (Te)$	7.4	40	544.35	Eutectic
$L \leftrightarrow Te$		0	449.55	Melting

**Table 2.** Crystallographic information for Sb-Te phases relevant in this study

Phase	Space group	Structure type	Lattice parameters (Å)	References
Sb <sub>48</sub> Te <sub>9</sub>	<i>R</i> -3 <i>m</i> (166)	Own	<i>A</i> = 4.293, <i>c</i> = 109.107	[11]
Sb <sub>4</sub> Te	<i>P</i> -3 (143)	Own	<i>a</i> = 4.289, <i>c</i> = 28.876	[12]
Sb <sub>8</sub> Te <sub>3</sub>	<i>R</i> -3 <i>m</i> (166)	Own	<i>a</i> = 4.280, <i>c</i> = 64.220	[9]
Sb <sub>2</sub> Te	<i>P</i> -3 <i>m</i> 1 (156)	Own	<i>a</i> = 4.277, <i>c</i> = 17.612	[11]
Sb <sub>4</sub> Te <sub>3</sub>	<i>R</i> -3 <i>m</i> (166)	Own	<i>a</i> = 4.272, <i>c</i> = 83.309	[13]
SbTe	<i>P</i> -3 <i>m</i> 1 (156)	Own	<i>a</i> = 4.269, <i>c</i> = 24.050	[14]
Sb <sub>2</sub> Te <sub>3</sub>	<i>R</i> -3 <i>m</i>	Bi <sub>2</sub> Te <sub>3</sub>	<i>a</i> = 4.2674, <i>c</i> = 30.450	[15]

showing one broad phase field  $\delta$  (11–60 at.% Te). They verify only one peritectic reaction ( $L + (\text{Sb}) \leftrightarrow \delta$ , 11 at.% Te, 550 °C), and they conclude that the two distinct phases found by Abrikosov<sup>[8]</sup> could be metastable compounds. Combined with the phase diagram of Hansen and Anderko,<sup>[19]</sup> Brown and Lewis<sup>[18]</sup> suggest the liquidus line in the phase diagram. A reinvestigation, especially of the liquidus and solidus in the range from 0 to 60 at.% Te, was done by Kim and Chao.<sup>[20]</sup> They found, through electron microprobe analysis, a variety of compositions between 20 and 60 at.% Te. They came to the conclusion that the solidus region (20–60 at.% Te) remains uncertain, but they do not support the suggestion of two distinct single phase fields by other authors. Last but not least, the suggestion of various layered superstructures was further investigated in thin film deposition studies by Kifune et al.<sup>[11, 12]</sup> They conclude that only one single phase field exists between Sb and Sb<sub>2</sub>Te<sub>3</sub>. The proposed range, 11.5–60 at.% Te includes the composition of Sb<sub>2</sub>Te<sub>3</sub> as part of the single-phase field.

In summary, there are considerable differences and uncertainties in the description of Sb-Te. Many experimental results suggest that the currently accepted phase diagram version by Ghosh<sup>[7]</sup> requires revision, but there is no consensus on the type of revision among recent authors. In the current work we present new experimental data for the heavily discussed Sb-rich part of Sb-Te, which allow to understand most of the findings of previous authors and, at the same time, delivers a new interpretation of the binary phase equilibria between Sb and Sb<sub>2</sub>Te<sub>3</sub>.

## 2 Experimental

More than 30 samples were prepared from lumps of pure Sb (Cominco Electronic Materials, 99.999 %) and Te (Johnson & Matthey, 99.999 %) (Alfa Aesar, 99.99%). Calculated amounts of the elements were weighed to an accuracy of  $\pm 0.5$  mg using a semi-micro balance. Total weights were 1000 mg for sample series 1, and 500 mg for the series 1.5 and 2, respectively. As arc melting was not possible due the high vapor pressure of Sb and Te, the weighed elements were placed into quartz glass tubes

(diameter 8 mm) which were evacuated, flushed with Ar for three times, and finally sealed under a dynamic vacuum better than  $8 \cdot 10^{-3}$  mbar. For homogenization the sealed phials were heated in a H<sub>2</sub>/O<sub>2</sub> flame until the entire sample was liquid. Samples of the series 1 were annealed directly after this initial homogenization step. However, as many of these samples were not completely equilibrated after heat treatment, samples of series 1.5 and 2 were powdered after initial melting, pressed into pellets of 5 mm diameter using a hydraulic press, resealed under vacuum and then annealed. After annealing in a muffle furnace at 520 °C for 2 weeks, samples were quenched in cold water and separated into several pieces used for further analysis.

Metallographic samples were prepared by embedding a representative part of each sample in electrically conducting phenolic hot mounting resin (PolyFast, Struers). These samples were then ground with abrasive SiC-paper in several steps and finally polished with Al<sub>2</sub>O<sub>3</sub>-powder of 1 and 0.3  $\mu\text{m}$  grain size. Metallographic samples were initially checked using a reflected light microscope (Zeiss Axiotech 100) operated in bright field, dark field and polarization mode. Subsequently, scanning electron microscopy was performed using a Zeiss Supra VP electron microscope operated with an acceleration voltage of 20 kV. Imaging was done using secondary electrons (SE) as well as back scattered electrons (BSE). As the atomic number of Te and Sb differs only by 1, the observed chemical (mass) contrast in BSE mode was insufficient and often outperformed by crystallographic orientation contrast. Therefore, it was necessary to measure a large number of points to check for homogeneity during quantitative analysis. For this, an energy dispersive detector (EDX) detector was used. Energy calibration was done with a Co standard and the characteristic x-ray lines used for quantitative analysis were calibrated using pure elemental standards of Tellurium and Antimony.

X-ray powder diffraction was used to determine and refine crystal structures. Representative parts of the samples were powdered with a WC mortar and the powder was fixed on a zero-background silicon single crystal sample holder using a thin layer of grease. The powder diffractometer (D8, ADVANCE, Bruker) was operated in Bragg-

Brentano pseudo focusing mode with  $\theta/2\theta$  geometry. Detector for all measurements was a one-dimensional silicon strip detector (Lynxeye). All samples were measured for 1 hour with an acceleration voltage of 40 kV and a beam current of 40 mA. Initial qualitative phase identification as well as Rietveld refinements were done using the Topas software.<sup>[21]</sup> For further investigations of patterns containing incommensurately modulated structures, the software Jana2000<sup>[22]</sup> was used.

A DTA/DSC 404 F1 Pegasus instrument (Netzsch) was used to determine the thermal reactions over the entire investigated composition range. Pieces of approximately 100 mg weight were sealed into evacuated quartz glass sample holders in order to avoid evaporation during DTA measurements. A sample of 100 mg Zr sealed in a quartz glass sample holder served as reference material. Each sample was measured for two heating- and cooling-circles using a heating rate of 5 K min<sup>-1</sup>. Measurements were started at room temperature and the maximal temperature was set between 600 and 670 °C, depending on the anticipated liquidus temperature of the specific sample. Temperature calibration of the Pt/Pt10%Rh thermocouples was done by acquiring the melting temperature of the pure elements Sn, Zn, Te, Sb, Ag and Au.

### 3 Results and Discussion

Compositions and selected experimental results for 27 samples prepared in the Sb-Te system are listed in Table 3. It contains 3 homogeneous bulk annealed samples (1D–1F), followed by two series of pressed powder samples. The 1.5 series (1.5 A–1.5 J) was prepared at the same nominal compositions as in series 1, while samples of series 2 (2A–2N) were prepared to cover additional nominal compositions. In the following discussion we exclusively use the designation “ $\gamma$ ” for all phase compositions found between pure Sb and Sb<sub>2</sub>Te<sub>3</sub>, as our discussion will show that the split into two different phases  $\gamma$  and  $\delta$ , proposed in the assessment of Ghosh<sup>[7]</sup> is not in line with the presented results.

#### 3.1 Results for Sample Series 1 (Bulk Annealing)

Most of the samples of series 1 were inhomogeneous due to the method of preparation and are therefore not listed in Table 3. This is reflected by a high standard deviation of measured phase compositions, and by the presence of non-equilibrium pure Sb in samples 1A–1C. The remarkable exceptions are samples 1D to 1F which were found to be homogeneous with only small local deviations from the mean phase composition. This is most likely due to the specific melting behaviour in this composition area, which

will be discussed in section 3.3. The microstructure of sample 1B (nominal composition: 82% Sb) is shown in Figure 2, left. Small grains of pure Sb are surrounded by obvious diffusion zones embedded in a matrix of  $\gamma$ -phase with quite inhomogeneous composition. Note, that the different colours of  $\gamma$ -grains are due to different crystallographic orientation and do not reflect the composition differences.

An EDX line scan was performed along the plotted line and the resulting composition curve is shown in Fig. 2, left. It is interesting to note, that the experimental composition results for the  $\gamma$ -phase, although determined from inhomogeneous samples, clearly contradict the literature phase boundary of  $\gamma$  in the assessment of Ghosh.<sup>[7]</sup> According to Ghosh, the Sb-rich boundary of  $\gamma/\delta$  phase field is found at 16.4 at.% Te, however experimental results in the current study suggest a significantly lower value. To estimate this phase boundary, we evaluated line scans of samples 1A, 1B and 1C for compositions in local equilibrium with pure Sb (example: Fig. 2, right). This evaluation yielded a preliminary phase boundary at  $12 \pm 1$  at.% Te ( $88 \pm 1$  at.% Sb).

Powder XRD was performed for all samples, despite the inhomogeneity observed in SEM. A reliable structure refinement was not possible for these samples, except for the two largely homogeneous samples 1D and 1E which were refined with the structural models of the reported superstructures Sb<sub>8</sub>Te<sub>3</sub> and Sb<sub>2</sub>Te, respectively. A graphical representation of the powder pattern and refinement result for sample 1E is shown in Fig. 3. The agreement of measured and refined pattern is generally good, but a careful evaluation of the diffraction line positions revealed unexpected differences for most of the minor intensity lines. The very same behaviour was also found for all other samples, but to a much larger extent. The fact that it was generally impossible to refine consistent lattice parameters for any of the samples within the series, raised some doubt regarding the general structural features within this phase field. An incommensurate modulation of a relatively simple structural model based on the As-type crystal structure appeared to be a possible solution for this problem of lattice parameter determination. However, it was decided to not try any advanced structure refinement with these inhomogeneous sample series, but rather re-synthesize the whole series.

#### 3.2 Results for Series 1.5 and 2 (Annealing of Pressed Powder Pellets)

Sample series 1.5 and 2 were found to be homogeneous after annealing, evidenced by only small variation of phase compositions measured by SEM/EDX (compare Table 3). SEM results clearly show the existence of one extended

**Table 3.** Experimental phase compositions and cell parameters for Sb-Te samples

Sample [nom. comp at.% Sb/Te]	Annealing	Comment	XRD		EDX
			Phase	Lattice parameters, Å, $\gamma_q^*$	Sb, at.%
1D [74/26]	Bulk, 520°, 2 weeks		“Sb <sub>8</sub> Te <sub>3</sub> ” = $\gamma$	$a = 4.280, c = 64.220$ $a = 4.280, c = 5.839, \gamma_q = 1.358$	$74.56 \pm 0.9$
1E [70/30]	Bulk, 520°, 2 weeks		“Sb <sub>2</sub> Te” = $\gamma$	$a = 4.277, c = 17.612$ $a = 4.277, c = 5.870, \gamma_q = 1.338$	$70.23 \pm 0.3$
1F [66/34]	Bulk, 520°, 2 weeks		$\gamma$	$a = 4.273, c = 5.887, \gamma_q = 1.322$	$66.70 \pm 1.4$
1.5 Beta [94/6]	Powder, 520°, 2 weeks		Sb $\gamma$	$a = 4.308, c = 5.637$ $a = 4.302, c = 5.721, \gamma_q = 1.439$	100 $88.2 \pm 0.2$
1.5 Alpha [90/10]	Powder, 520°, 2 weeks		Sb $\gamma$	$a = 4.308, c = 5.637$ $a = 4.301, c = 5.715, \gamma_q = 1.436$	100 $88.8 \pm 0.4$
1.5A [86/14]	Powder, 520°, 2 weeks		“Sb <sub>48</sub> Te <sub>9</sub> ” = $\gamma$	$a = 4.293, c = 109.107$ $a = 4.293, c = 5.742, \gamma_q = 1.418$	$86.0 \pm 0.4$
1.5B [82/18]	Powder, 520°, 2 weeks		“Sb <sub>4</sub> Te” = $\gamma$	$a = 4.288, c = 28.876$ $a = 4.288, c = 5.775, \gamma_q = 1.400$	$81.9 \pm 0.4$
1.5C [78/22]	Powder, 520°, 2 weeks		$\gamma$	$a = 4.282, c = 5.805, \gamma_q = 1.375$	$78.1 \pm 0.4$
1.5G [62/38]	Powder, 520°, 2 weeks		$\gamma$	$a = 4.270, c = 5.916, \gamma_q = 1.299$	$65.5 \pm 1.2$
1.5H [58/42]	Powder, 520°, 2 weeks		“Sb <sub>4</sub> Te <sub>3</sub> ” = $\gamma$	$a = 4.272, c = 83.309$ $a = 4.269, c = 5.948, \gamma_q = 1.280$	$57.9 \pm 0.8$
1.5I [54/46]	Powder, 520°, 2 weeks		$\gamma$	$a = 4.273, c = 5.887, \gamma_q = 1.322$	$53.7 \pm 1.2$
1.5J [50/50]	Powder, 520°, 2 weeks		“SbTe” = $\gamma$	$a = 4.269, c = 24.050$ $a = 4.267, c = 5.980, \gamma_q = 1.260$	$50.5 \pm 1.3$
2 Alpha [92/8]	Powder, 520°, 2 weeks		Sb $\gamma$	$a = 4.308, c = 5.637$ $a = 4.302, c = 5.711, \gamma_q = 1.440$	100 $88.8 \pm 0.2$
2A [88/12]	Powder, 520°, 2 weeks		$\gamma$	$a = 4.295, c = 5.720, \gamma_q = 1.425$	$87.8 \pm 0.3$
2B [84/16]	Powder, 520°, 2 weeks		$\gamma$	$a = 4.291, c = 5.758, \gamma_q = 1.411$	$83.3 \pm 0.4$
2C [80/20]	Powder, 520°, 2 weeks		$\gamma$	$a = 4.286, c = 5.791, \gamma_q = 1.385$	$79.5 \pm 0.2$
2D [76/24]	Powder, 520°, 2 weeks		$\gamma$	$a = 4.281, c = 5.822, \gamma_q = 1.365$	$75.9 \pm 0.2$
2E [72/28]	Powder, 520°, 2 weeks		$\gamma$	$a = 4.278, c = 5.850, \gamma_q = 1.344$	$71.7 \pm 0.2$
2F [68/32]	Powder, 520°, 2 weeks	SEM & DTA only	$\gamma$	Not determined	$67.8 \pm 0.2$
2G [64/36]	Powder, 520°, 2 weeks	SEM & DTA only	$\gamma$	Not determined	$64.2 \pm 0.2$
2H [60/40]	Powder, 520°, 2 weeks	SEM & DTA only	$\gamma$	Not determined	$59.4 \pm 0.4$
2I [56/44]	Powder, 520°, 2 weeks	SEM & DTA only	$\gamma$	Not determined	$55.9 \pm 0.3$
2J [52/48]	Powder, 520°, 2 weeks	SEM & DTA only	$\gamma$	Not determined	$51.5 \pm 0.3$
2K [47/53]	Powder, 520°, 2 weeks		$\gamma$	$a = 4.264, c = 6.036, \gamma_q = 1.229$	$46.6 \pm 0.8$
2L [40/60]	Powder, 520°, 2 weeks		Sb <sub>2</sub> Te <sub>3</sub>	$a = 4.263, c = 30.467$	$39.6 \pm 0.2$
2M [42/58]	Powder, 520°, 2 weeks	SEM & DTA only	$\gamma$	Not determined	$43.1 \pm 1.2$
			Sb <sub>2</sub> Te <sub>3</sub>	Not determined	$40.8 \pm 0.2$

\* $\gamma_q$  is the component of the incommensurate  $\mathbf{q}$ -vector ( $\mathbf{q} = \gamma_q \cdot \mathbf{c}^*$ )

single-phase field ( $\gamma$ ) ranging from 88.6 at.% Sb (average value determined from three two-phase samples) to 43.1% Sb (determined from one two-phase sample). The Sb-rich phase boundary is in very good agreement with the estimation based on evaluation of the local equilibria in sample series 1, and it also agrees with the phase boundary suggested by Brown and Lewis<sup>[18]</sup> and Kifune et al.<sup>[11, 12]</sup>

However, it differs significantly from the broadly accepted assessment from Ghosh<sup>[7]</sup> (83 at.% Sb). The Te-rich phase boundary of  $\gamma$ , on the other hand, is not in line with Kifune et al.,<sup>[11, 12]</sup> as these authors suggested a continuous extension of the phase to Sb<sub>2</sub>Te<sub>3</sub>, but it also differs significantly from the phase boundary suggested by Ghosh<sup>[7]</sup> (51 at.% Sb).



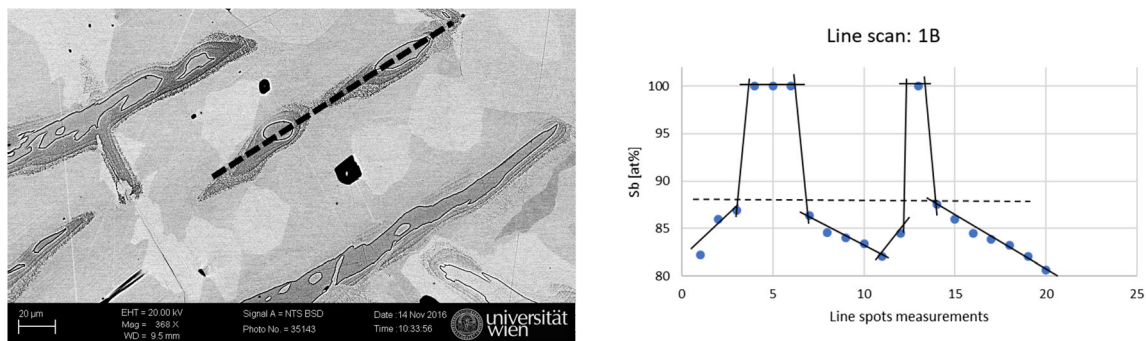


**Fig. 2.** Left: BSE image of the microstructure of sample 1B showing non-equilibrium Sb grains surrounded by a diffusion zone in the  $\gamma$ -phase with varying Sb-content, embedded in a matrix of more Te-rich

$\gamma$ -phase. The black line indicates the direction of a performed EDX line scan. Right: Line scan result for this sample with extrapolated local equilibrium phase boundary plotted as dashed line

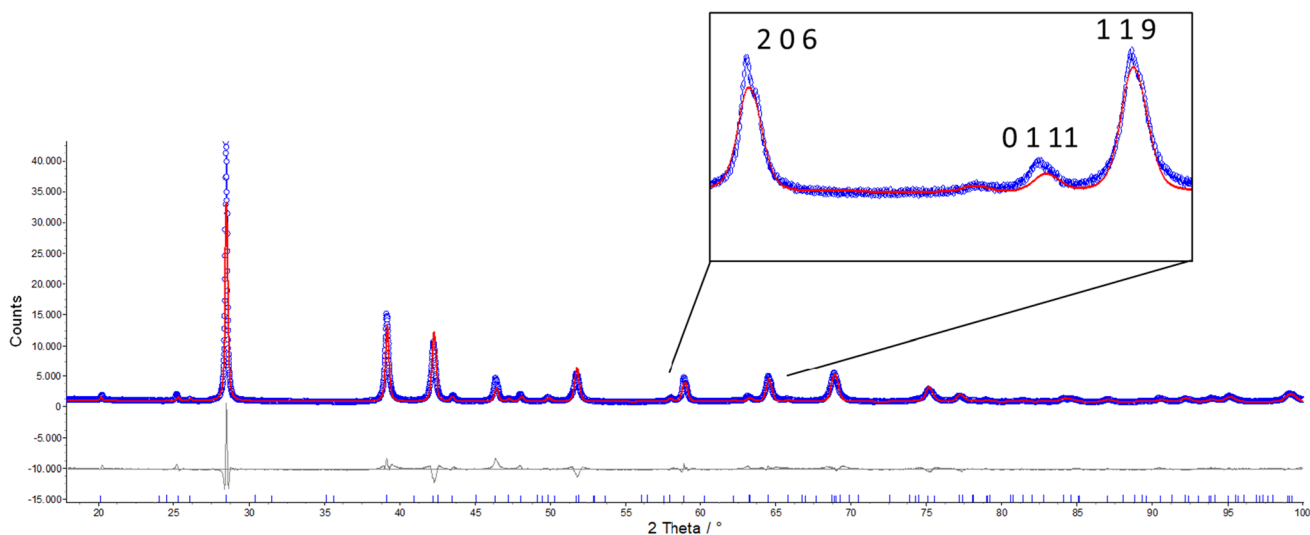


**Fig. 3.** Experimental powder XRD pattern of Sample 1E refined with the structural model of  $\text{Sb}_2\text{Te}$ . Blue circles: experimental data, red line: theoretical pattern observed by Rietveld refinement, grey line below: difference curve. The magnified and indexed insert shows, that

the positions of minor lines (eg 0 1 11) were not reproduced well by the model; a first indication for a possible incommensurate modulation (Color figure online)

Results from powder XRD showed continuous variation of diffraction line positions in a relatively simple diffraction pattern. It was possible to refine some of the patterns using different superstructure models (compare Table 3), but with similar problems for some minor line positions as shown in Fig. 3. For the most patterns, refinement with a classical crystal structure model was not possible due to the impossibility to obtain consistent lattice parameters using the commensurate structure models from literature (Table 2).

An analysis of these structures revealed common crystallographic features (see also Fig. 4 for a collection of relevant superstructures):

- All are commensurate superstructures based on the Sb-structure with sometimes very long  $c$ -parameters.

- They are built from atomic layers perpendicular to the crystallographic  $c$ -axis, where each layer contains only one atomic species.
- Five alternating Sb- and Te-layers form a  $\text{Sb}_3\text{Te}_2$ -building block.
- The stoichiometry of each compound is maintained through the insertion of the proper number of Sb-layers in between the  $\text{Sb}_3\text{Te}_2$ -blocks.

As will be shown in the following, these observations revealed remarkable structural similarities to compounds in the Sb-Sn system,<sup>[23–26]</sup> which has an incommensurate crystal structure (compare Lidin et al. and Noren et al.<sup>[23, 24]</sup>)

In a recent study (see Refs. 25, 26 for details), numerous misconceptions about the Sb-Sn system could be clarified. Besides the introduction of a compound  $\text{Sb}_3\text{Sn}_4$  (formed

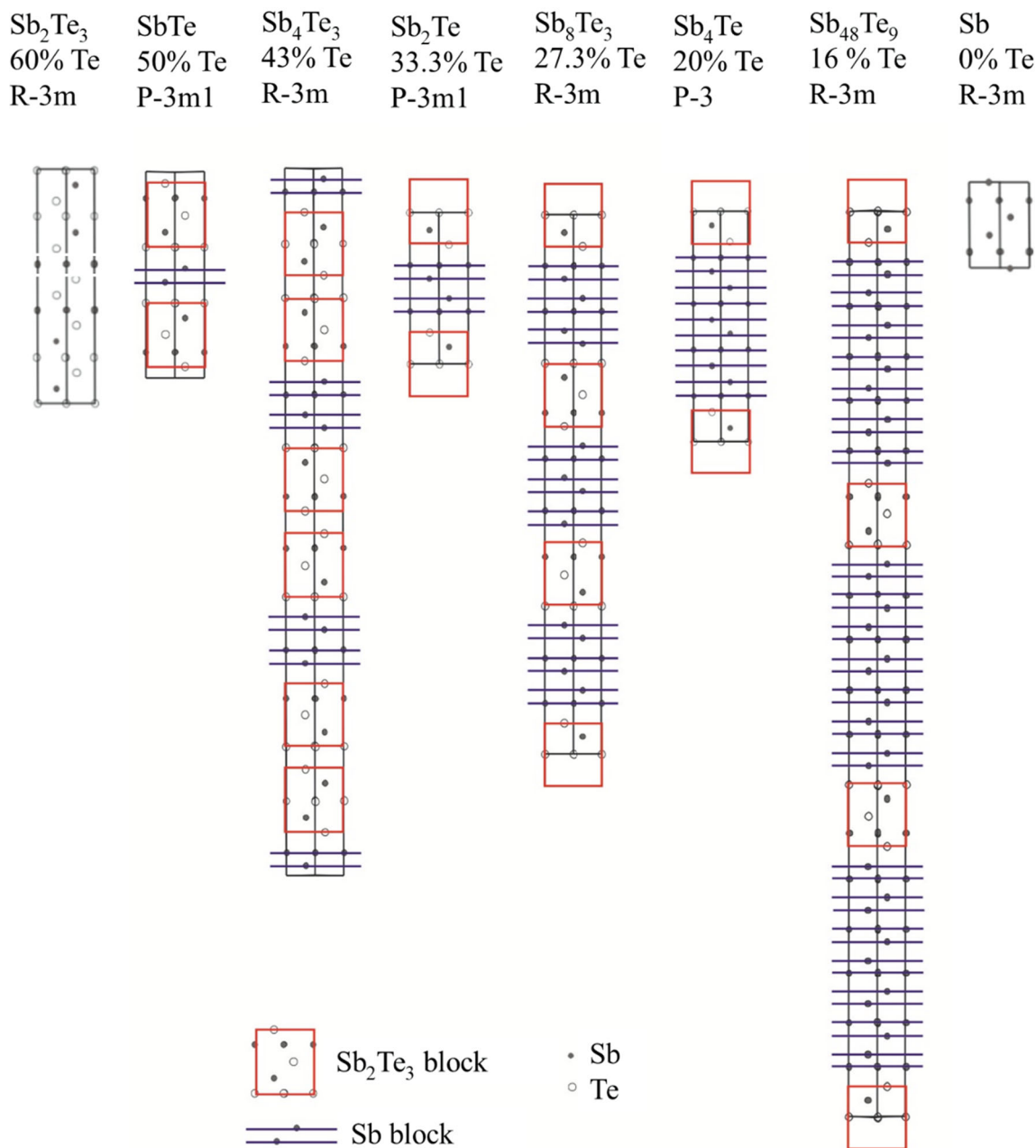


**Fig. 4.** Unit cells of various superstructures proposed for the composition range 0–60 at.% Te in the Sb–Te system. The structures are based on alternate stacking of  $\text{Sb}_2\text{Te}_3$ - and Sb-like blocks (see insert below).  $\text{Sb}_2\text{Te}_3$  (left) and Sb (right) are considered as end members of the series

peritectically at 326 °C), the most important findings with relevance to the present work are:

- The structure of the compound  $\text{SbSn}$  is incommensurately modulated<sup>[23, 24]</sup>
- It is built from atomic layers perpendicular to the crystallographic  $c$ -axis
- Seven alternating Sn- and Sb-layers form  $\text{Sb}_3\text{Sn}_4$ -blocks
- These layers are separated by the proper amounts of Sb-layers corresponding to the stoichiometry.

The structure of  $\text{Sb}_3\text{Sn}_4$  was derived from this model by eliminating all additional Sb-layers. It is composed of three  $\text{Sb}_3\text{Sn}_4$ -blocks and is isotypic to  $\text{P}_3\text{Sn}_4$  (see also Stegherr.<sup>[27]</sup> This very close relationship between the two Sb–Sn compounds was noticed by the fact that the  $\gamma_q$ -component ( $\mathbf{q} = \gamma_q \cdot \mathbf{c}^*$ ) of the incommensurate  $\mathbf{q}$ -vector assumed the rational value of 9/7 at the  $\text{Sb}_3\text{Sn}_4$ -composition, which hints at a commensurate super structure.<sup>[25, 26]</sup>  $\gamma_q$  remains constant over the small homogeneity range of  $\text{Sb}_3\text{Sn}_4$  but rises significantly within the broad  $\text{SbSn}$ -homogeneity range. Interestingly, at the approximate Sb-rich

limit of SbSn, it assumes a value of  $19/14$  (as compared to  $9/7 = 18/14$  at the Sn-rich side), and reaches  $21/14 = 1.5$  for pure Sb. This means, the Sb-structure itself can be described as an incommensurate superstructure of a rhombohedral cell in trigonal setting with  $\gamma_q = 1.5$ . However, at  $\gamma_q = 20/14$ , no hint for the existence of a further structure has been obtained. Instead, there is a broad two-phase field [SbSn + (Sb)], which is explained by Lidin et al. and Noren et al.<sup>[23, 24]</sup> by a loss of correlation between the  $Sb_3Sn_4$ -building blocks through the insertion of “too many” Sb-layers (in the sense that a sufficiently large number of Sb-layers in fact constitutes a Sb-grain and therefore a second phase). For the sake of completeness, it has to be mentioned that incommensurability is caused by a distortion of the atomic arrangement.

Although no incommensurability has been mentioned in the literature for the Sb-Te system, the mentioned striking crystallographic similarities to Sb-Sn (notably the layer-wise atom arrangement, the existence of  $Sb_3Sn_4$  or  $Sb_3Te_2$  building blocks, insertion of additional Sb-layers) suggested attempts to verify a possible incommensurate modulation in the Sb-Te system.<sup>[25, 26]</sup>

Using the experience from the Sb-Sn system as a starting point, the XRD recordings from numerous samples listed in Table 3 were refined using the software JANA2006, which allows the introduction of incommensurability in the crystal structure. Background, average cell and profile of the main reflexes were refined first, then incommensurability was introduced to determine  $\gamma_q$ , and eventually peak intensities were refined using atom positions. Lidin et al. and Noren et al.<sup>[23, 24]</sup> mention that Sb and Sn could be distinguished in the XRD-refinements despite their similar scattering power, because they form sub-lattices with different rigidity. For the refinement of the

powder patterns in the present work, the scattering function of Sb was used for all atom positions (i.e., no distinction of Sb and Te was made). For this reason, all positions were described by the single position with coordinates (0,0,0).

In the evaluation of the XRD patterns, a key role is assumed by the weak satellite reflexes. Commensurability and incommensurability can be distinguished by the value of  $\gamma_q$ , whether it is rational or irrational. An important further criterion noticed in Sb-Sn was not so much the existence of the satellites alone (they exist for commensurate and incommensurate crystal structures), but the composition dependency of their angular position in SbSn with respect to the main reflexes, which is of course one consequence of a change in  $\gamma_q$ .

In the Sb-Te system, a completely similar observation was made for the  $\gamma$ -phase: in Fig. 5, we show a collection of powder patterns of phase-pure samples showing a continuous variation of the diffraction pattern in combination with significant shifts of weak satellite reflexes. Refinement results obtained with JANA are given in Table 3 for a broad variety of samples containing the  $\gamma$ -phase. It was possible to refine the  $\gamma$ -phase using the incommensurate model described above in all cases. The model parameters are given in Table 4. For those samples, where refinements with commensurate superstructure models were possible, both refinement results are given for comparison (samples 1D, 1E, 1.5A, 1.5B, 1.5H, 1.5J). These samples have compositions near the ideal superstructure compositions leading to reasonable agreement with the ideal structure pattern and (using the modulated model) to  $\gamma_q$  close to the respective rational number.

The variation of  $\gamma_q$  and lattice parameters with the composition within the  $\gamma$ -phase is shown in Figure 6. For comparison, parameters for pure Sb and  $Sb_2Te_3$  refined

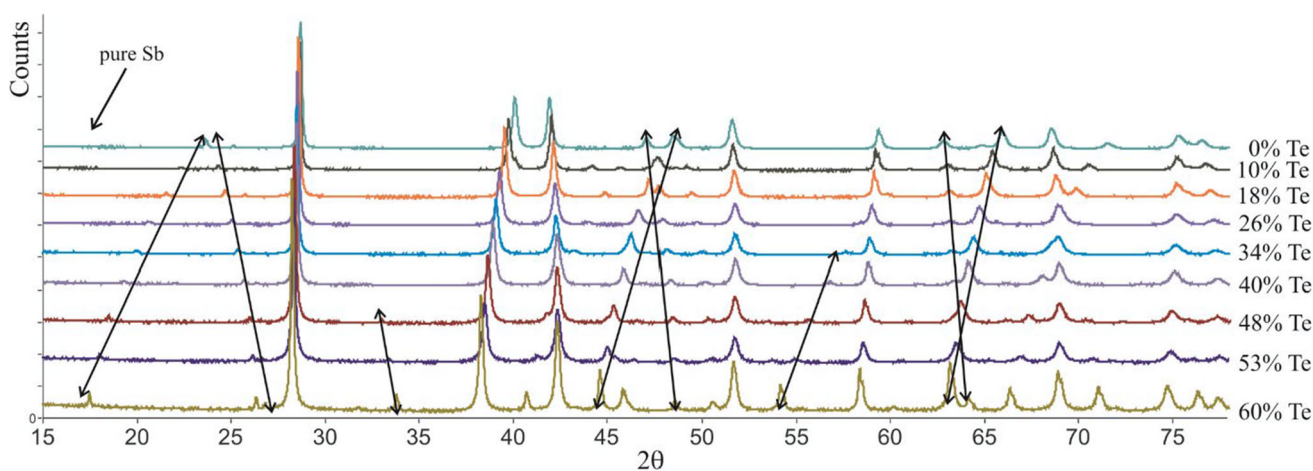


**Fig. 5.** A collection of powder patterns of phase-pure samples showing a continuous variation of the diffraction pattern. The obtained diffraction patterns show clear evidence for a continuously modulated crystal structure; emphasized by the strong variation of the

angular position of weak satellite reflections (black arrows). Patterns of pure Sb (0 at.% Te) and  $Sb_2Te_3$  (60 at.% Te), situated outside of the  $\gamma$  single-phase field are shown for comparison



**Table 4.** Structure model refined for the  $\gamma$ -phase showing values at the two boundary compositions

at.% Te	Space group	$a$ , Å	$c$ , Å	$\gamma_q$ -vector	$x, y, z$
12	R-3m(0,0, $\gamma$ )	4.295 ( $\pm 0.77 \cdot 10^{-4}$ )	5.720 ( $\pm 2.13 \cdot 10^{-4}$ )	1.425	0,0,0
53	R-3m(0,0, $\gamma$ )	4.264 ( $\pm 1.35 \cdot 10^{-4}$ )	6.036 ( $\pm 2.73 \cdot 10^{-4}$ )	1.229	0,0,0

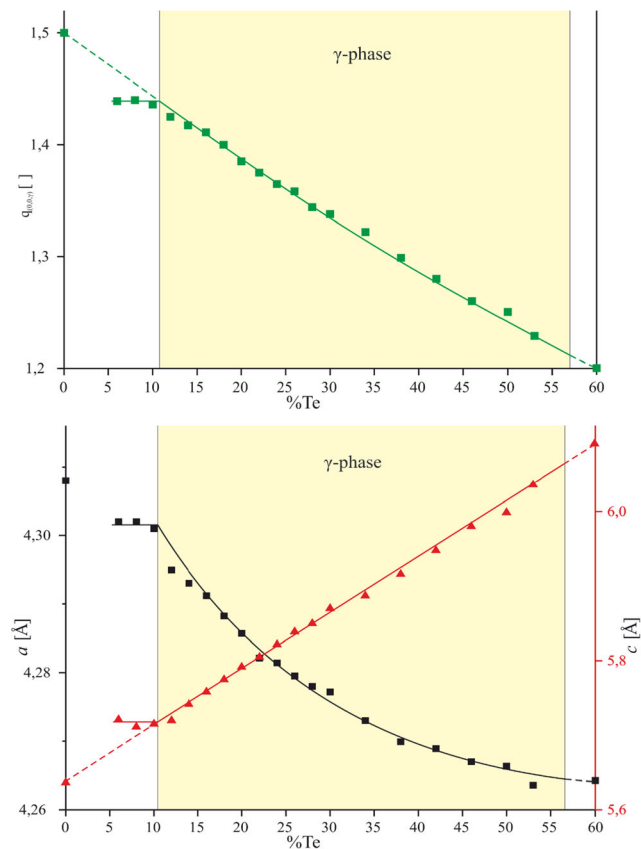


**Fig. 6.** Variation of  $\gamma_q$  (top) and basic cell parameters (down) of the  $\gamma$ -phase with the composition, refined in the incommensurate structural model discussed in the text. The homogeneity range of the phase is highlighted by the yellow background. Parameters for pure Sb and  $\text{Sb}_2\text{Te}_3$  refined with the same model are shown for comparison (Color figure online)

with the very same model are also shown. The variation is smooth and consistent throughout the entire single-phase field (88.6–43.1 at.% Sb). We did not find any evidence for a two-phase field in this area in SEM or EDX data. As expected, the parameter  $\gamma_q$  varies linearly between Sb (1.5 = 3/2) and  $\text{Sb}_2\text{Te}_3$  (1.2 = 5/6), being the respective end members of the series. Surprisingly, even the lattice parameters of the basic cell extrapolate well to  $\text{Sb}_2\text{Te}_3$ , despite the intermediate small two-phase gap. Extrapolation of the  $\gamma$ -phase lattice parameters to Sb is much worse, for the  $a$ -parameter.

### 3.3 DTA Results and Phase Diagram

A total number of 26 well equilibrated samples were investigated by DTA in order to determine the thermal reactions in the composition range 0–60 at.% Te. Samples were essentially taken from series 1.5 and 2, but also include the three homogeneous samples 1D–1F. The composition area of the single-phase field  $\gamma$  was covered by a fine raster of samples. Additionally, the phase  $\text{Sb}_2\text{Te}_3$  and the two-phase fields ( $\text{Sb} + \gamma$ ) and ( $\gamma + \text{Sb}_2\text{Te}_3$ ) are covered by samples.

Results of these measurements are listed in Table 5 and are included in Fig. 7 which shows the phase equilibria between Sb and  $\text{Sb}_2\text{Te}_3$  according to our evaluation. It must be stated that the scattering of measured reaction temperatures is relatively high, due to experimental difficulties observed in the system Sb–Te. First, solidus temperatures and invariant reaction temperatures occur in a very small temperature interval of less than 15 K, so the separation of thermal effects is often challenging. Secondly, it was necessary to measure the samples in sealed and evacuated quartz-glass ampoules to suppress evaporation of the volatile components Sb and Te during measurement. These ampoules are heavier and have less thermal conductivity compared to thin-walled standard crucibles made from alumina, and they are therefore reducing the quality of obtained data.

Data listed in Table 5 are the average values of first and second heating cycle, except for a few cases which only allowed the evaluation of one of the curves. As considerable supercooling is observed throughout the system, the cooling effects were not evaluated. Our data confirm the congruent melting point minimum in the  $\gamma (= \delta)$ -phase, reported in all available phase diagram versions, and they also agree with the very flat course of the solidus line of  $\gamma$  reported in other works. However, as we do not confirm the existence of two separate phase fields  $\gamma$  and  $\delta$ , we report different invariant reactions. According to our findings, the  $\gamma$  phase shows a congruent melting point minimum at 535 °C and 30 at.% Sb, and two peritectic melting points at 547 °C/15 at.% Sb and 547.5/52 at.% Sb, respectively. The course of liquidus temperatures observed in our work extrapolates well to the literature melting point of pure Sb. The melting point of  $\text{Sb}_3\text{Te}_2$  found in this study (612 °C) is about 5 K lower than the value reported in Ref. [7].

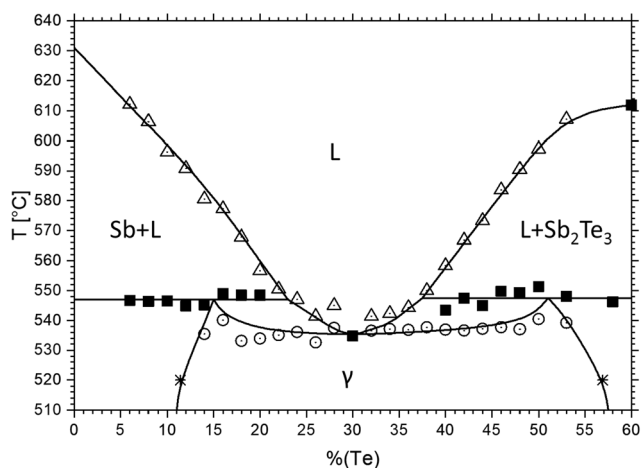


**Fig. 7.** Phase diagram Sb-Te in the composition range between Sb and  $\text{Sb}_2\text{Te}_3$  according to the current work. Black squares: invariant arrests (DTA); white triangles: liquidus (DTA); white circles: solidus (DTA); asterisks: phase boundary of the  $\gamma$ -phase at 520 °C (SEM/EDX)

A list of invariant reaction temperatures and corresponding phase compositions is given in Table 6. The Sb-rich peritectic agrees remarkably well with the assessment of Ghosh, while the congruent melting point minimum was found about 10 K lower than proposed there. The reaction temperature of the Te-rich peritectic agrees again very well with the peritectic decomposition of  $\delta$  by Ghosh,<sup>[7]</sup> while we did not find any evidence for a third peritectic around 557 °C, as proposed there.

#### 4 Conclusions

The difficulties preventing full understanding of phase equilibria in the Sb-rich part of Sb-Te up to now, are due to several challenges in this specific system.

- Sluggish reaction kinetics due to large atoms and moderate annealing temperatures hinder easy equilibration.
- Powder patterns are simple at the first sight, but hard to understand on detailed investigation, triggering the

development of many different superstructure models and causing doubts about the number of phases present in the system.

- Thermal reactions occur in a very small temperature window around 540 °C, making it difficult to sort out the number and nature of invariant reactions.

In this study we present new experimental data contributing to the better understanding of the system Sb-Te and we suggest a new version of the phase diagram in the composition range between 0 and 60 at.% Te. By using a fine raster of well equilibrated samples annealed at 520 °C it was possible to rule out the existence of any extended two-phase field between 11.4 and 56.9 at.% Te. By successfully applying a structural model in the (3 + 1)-dimensional super-space group  $R\text{-}3m(0,0,\gamma)$  to all single phase samples in this area, it was furthermore possible to rationalize the crystal structure of this single-phase field. It is important to state, that this structural model is not in conflict with crystalline superstructures reported earlier,<sup>[9, 11–14]</sup> as these superstructures can be understood as commensurate parts of the single-phase field characterized by rational values of the  $\gamma_a$ -component of the modulation vector, as far as the cell metrics is concerned. A more detailed view on the distribution of Sb and Te was not possible based on powder data, as very similar scattering factors of these two elements do not allow separation. Evaluation of DTA experiments furthermore allowed to propose a new binary reaction scheme between 0 and 60 at.% Te, including a congruent melting point minimum of  $\gamma$  and the two peritectic reactions  $L + (\text{Sb}) \leftrightarrow \gamma$  and  $L + \text{Sb}_2\text{Te}_3 \leftrightarrow \gamma$ .

The extended single-phase field  $\gamma$  was confirmed for the annealing temperature of 520 °C, only about 15 K below the melting point minimum of the phase. The further development of this single-phase field at lower temperatures is not known up to now. Long term-annealed samples are necessary to investigate the possibility of the  $\gamma$ -phase decomposing into several stability islands around specific superstructure compositions at lower temperature.

**Table 5.** Thermal arrests obtained by DTA and their interpretation

Sample composition, at.% Te	Solidus, °C	Invariant, °C	liquidus, °C
6		546.7	612.2
8		546.4	606.3
10		546.5	596.3
12		544.8	590.8
14	535.4	545.1	580.6
16	540.1	549	577.3
18	533.1	548.4	567.8
20	533.9	548.4	556.7
22	535.1		550.5
24	536.1		547
26	532.6		541.4
28	537.5		545
30		534.8	
32	536.5		541.4
34	537.1		542.3
36	536.8		544.3
38	537.7		550
40	536.9	543.4	558.3
42	536.6	547.4	566.8
44	537.2	545	573.3
46	537.7	549.7	583.6
48	537	549.3	590.4
50	540.4	551.3	597.3
53	539.2	548	607.2
58		546.2	609.4
60		611.9	

**Table 6.** Invariant reaction temperatures and corresponding phase compositions according to this study

Reaction	Composition, at.% Te			Temp., °C	Reaction type
$L + (\text{Sb}) \leftrightarrow \gamma$	23	0	~ 15	$547 \pm 2$	Peritectic
$L \leftrightarrow \gamma$	30	30		535	Congruent
$L + \text{Sb}_2\text{Te}_3 \leftrightarrow \gamma$	37.5	59.2	~ 51	$547.5 \pm 3$	Peritectic
$L \leftrightarrow \text{Sb}_2\text{Te}_3$	60	60		612	Congruent

**Acknowledgment** The authors thank Stephan Puchegger and the Faculty Center for Nanostructure Research at the University of Vienna for help with the SEM/EDX measurements.

**Funding** Open access funding provided by University of Vienna.

**Open Access** This article is licensed under a Creative Commons Attribution 4.0 International License, which permits use, sharing,

adaptation, distribution and reproduction in any medium or format, as long as you give appropriate credit to the original author(s) and the source, provide a link to the Creative Commons licence, and indicate if changes were made. The images or other third party material in this article are included in the article's Creative Commons licence, unless indicated otherwise in a credit line to the material. If material is not included in the article's Creative Commons licence and your intended use is not permitted by statutory regulation or exceeds the permitted

use, you will need to obtain permission directly from the copyright holder. To view a copy of this licence, visit <http://creativecommons.org/licenses/by/4.0/>.

## References

1. T. Dankwort, A.-L. Hansen, M. Winkler, U. Schuermann, J.D. Koenig, D.C. Johnson, N.F. Hinsche, P. Zahn, I. Mertig, W. Bensch, and L. Kienle, Nanostructure, Thermoelectric Properties, and Transport Theory of V2VI3 and V2VI3/IV-VI Based Superlattices and Nanomaterials, *Phys. Status Solidi A*, 2016, **213**(3), p 662–671.
2. C. Kang, H. Wang, J.-H. Bahk, H. Kim, and W. Kim, Thermoelectric Materials and Devices, *RSC Nanosci. Nanotechnol. (Hierarch. Nanostruct. Energy Devices)*, 2015, **35**, p 107–141.
3. Y.T. Kim, and S.-I. Kim, Comparison of Thermal Stabilities Between Ge-Sb-Te and In-Sb-Te Phase Change Materials, *Appl. Phys. Lett.*, 2013, **103**(12), 121906.
4. N. Yamada, E. Ohno, K. Nishiuchi, N. Akahira, and M. Takao, Rapid-phase Transitions of GeTe-Sb<sub>2</sub>Te<sub>3</sub> Pseudobinary Amorphous Thin Films for an Optical Disk Memory, *J. Appl. Phys.*, 1991, **69**(5), p 2849–2856.
5. G. Sobon, Mode-Locking of Fiber Lasers using Novel Two-Dimensional Nanomaterials: Graphene and Topological Insulators [Invited], *Photonics Res.*, 2015, **3**(2), p 56–63.
6. G. Wang, X. Zhu, J. Wen, X. Chen, K. He, L. Wang, X. Ma, Y. Liu, X. Dai, Z. Fang, J. Jia, and Q. Xue, Atomically Smooth Ultrathin Films of Topological Insulator Sb<sub>2</sub>Te<sub>3</sub>, *Nano Res.*, 2010, **3**(12), p 874–880.
7. G. Ghosh, The Sb-Te (Antimony-Tellurium) System, *J. Phase Equilib.*, 1994, **15**(3), p 349–360.
8. N.K. Abrikosov, L.V. Poretzkaya, and I.P. Ivanova, The Antimony-Tellurium System, *Zh. Neorg. Khim.*, 1959, **4**, p 2525–2530.
9. L.E. Shelimova, O.G. Karpinskii, M.A. Kretova, V.I. Kosyakov, V.A. Shestakov, V.S. Zemskov, and F.A. Kuznetsov, Homologous Series of Layered Tetradymite-Like Compounds in the Sb-Te and GeTe-Sb<sub>2</sub>Te<sub>3</sub> Systems, *Inorg. Mater.*, 2000, **36**(8), p 768–775.
10. P.M. Imamov, and S.A. Semiletov, The Crystal Structure of the Phases in the Systems Bi-Se Bi-Te and Sb-Te, *Soviet Phys. Crystallogr.*, 1971, **15**(5), p 845–850.
11. K. Kifune, Y. Kubota, T. Matsunaga, and N. Yamada, Extremely Long Period-Stacking Structure in the Sb-Te Binary System, *Acta Cryst. B*, 2005, **61**(5), p 492–497.
12. K. Kifune, T. Fujita, T. Tachizawa, Y. Kubota, N. Yamada, and T. Matsunaga, Crystal Structures of X-Phase in the Sb-Te Binary Alloy System, *Cryst. Res. Technol.*, 2013, **48**(11), p 1011–1021.
13. P.F.P. Poudeu, and M.G. Kanatzidis, Design in Solid State Chemistry Based on Phase Homologies. Sb<sub>4</sub>Te<sub>3</sub> and Sb<sub>8</sub>Te<sub>9</sub> As New Members of the Series (Sb<sub>2</sub>Te<sub>3</sub>)<sub>m</sub>(.)<sub>1</sub>(Sb-2)<sub>n</sub>, *Chem. Commun.*, 2005, **21**, p 2672–2674.
14. M.M. Stasova, Crystal Structure of Bismuth Selenides and Bismuth and Antimony Tellurides, *J. Struct. Chem.*, 1967, **8**(4), p 584–589.
15. A.N. Mansour, W. Wong-Ng, Q. Huang, W. Tang, A. Thompson, and J. Sharp, Structural Characterization of Bi<sub>2</sub>Te<sub>3</sub> and Sb<sub>2</sub>Te<sub>3</sub> As a Function of Temperature Using Neutron Powder Diffraction and Extended X-ray Absorption fine Structure Techniques, *J. Appl. Phys.*, 2014, **116**(8), 083513.
16. C. Guo, C. Li, and Z. Du, Thermodynamic Re-modeling of the Sb-Te System Using Associate and Ionic Models, *J. Electron. Mater.*, 2014, **43**(11), p 4082–4089.
17. P. Eckerlin, and A. Stegherr, Zur Kenntnis der Phase im System Sb-Te, *Acta Cryst.*, 1966, **S21**, p A78.
18. A. Brown, and B. Lewis, The Systems Bismuth-Tellurium and Antimony-Tellurium and the Synthesis of the Minerals Hedleyite and Wehrlite, *J. Phys. Chem. Sol.*, 1962, **23**(11), p 1597–1604.
19. M. Hansen, and K. Anderko, *Constitution of Binary Alloys*. McGraw-Hill, New York, 1958.
20. W.-S. Kim, and G.Y. Chao, Phase Relations in the System Pt-Sb-Te, *Can. Mineral.*, 1990, **28**(3), p 675–685.
21. S. TOPAS, V4.2 Bruker AXS Inc., Karlsruhe, Germany (2009).
22. V. Petříček, M. Dušek, and L. Palatinus, Crystallographic Computing System JANA2006: General features, *Zeitschrift für Kristallographie Crystal. Mater.*, 2014, **229**(5), p 345–352.
23. S. Lidin, J. Christensen, K. Jansson, D. Fredrickson, R. Withers, L. Norén, and S. Schmid, Incommensurate Stibite—Order Made to Order, *Inorg. Chem.*, 2009, **48**(12), p 5497–5503.
24. L. Noren, R.L. Withers, S. Schmid, F.J. Brink, and V. Ting, Old Friends in a New Light: “SnSb” Revisited, *J. Solid State Chem.*, 2006, **179**(2), p 404–412.
25. C. Schmetterer, J. Polt, and H. Flandorfer, The Phase Equilibria in the Sb-Sn System—Part I: Literature Review, *J. Alloys Compds.*, 2017, **728**, p 497–505.
26. C. Schmetterer, J. Polt, and H. Flandorfer, The phase Equilibria in the Sb-Sn System—Part II: Experimental Results, *J. Alloys Compds.*, 2018, **743**, p 523–536.
27. A. Stegherr, A Three Component System of Tin-Antimony-Tellurium, *Philips Res. Rep.*, 1969, **6**, p 1–000.

**Publisher’s Note** Springer Nature remains neutral with regard to jurisdictional claims in published maps and institutional affiliations.